AIAA JOURNAL
Vol. 39, No. 12, December 2001

Multibody System Analysis Based on Hamilton's Weak Principle

Donald L. Kunz*
Old Dominion University, Norfolk, Virginia 23529-0247

The double pendulum, a simple system that exhibits complex dynamics, is used to demonstrate a method based on Hamilton's weak principle (HWP) for assembling and solving the maximum coordinate set equations for a multibody system. Results calculated using HWP are compared to a reference solution obtained by integrating the ordinary differential equations (ODE) in minimum coordinate set form. The HWP solution is shown to be comparable to the ODE solution in accuracy and computational efficiency. These results suggest an alternative architecture for multibody system analysis, which implements the maximum coordinate set form of the system equations, and a simple, efficient, and robust solution algorithm.

Nomenclature

f_1, f_2	=	displacement constraint function
g	=	gravity, m/s^2
g_1, g_2	=	momentum constraint function
H	=	Hamiltonian
l_1, l_2	=	pendulum rod length, m
m_1, m_2	=	pendulum bob mass, kg
p_1, p_2	=	momentum, kg · m · s
$\boldsymbol{Q}$	=	generalized force vector
q_1, q_2	=	momentum, kg · m · s
T	=	kinetic energy, kg · m^2 · s^2 or N · m
t	=	time, s
t_f	=	final time, s
t_i	=	initiation time, s
x_1, x_2, z_1, z_2	=	pendulum bob displacement, m
Δt	=	time step, s
$\delta()$	=	variation
θ_1, θ_2	=	pendulum bob angle, rad
λ_1, λ_2	=	Lagrange multipliers
μ_1, μ_2	=	Lagrange multipliers
$\boldsymbol{\xi}$	=	displacement vector
$\boldsymbol{\rho}$	=	momentum vector
ω_1, ω_2	=	pendulum angular velocity, rad/s

Superscripts

$\dot{}$	=	derivative with respect to time
$\bar{}$	=	value during a time step
$\hat{}$	=	value at one end of a time step

Introduction

MULTIBODY systems analysis (MSA) was primarily developed as a means for performing simulations of mechanisms using rigid bodies connected by joints. Since the development of the earliest MSA computer programs, numerous MSA programs have been made available commercially or have been developed for use as research codes. The two most widely used commercial programs are ADAMS[1] (Mechanical Dynamics, Inc.) and DADS[2] (Computer Aided Design Software, Inc.). Other commercial programs include Pro/MECHANICA MOTION (Parametric Technologies Corporation), SIMPACK[3] (DLR/INTEC Gmbh), Working Model (Knowledge Revolution, Inc.), DISCOS (Photon Research Associates), and TREETOPS (NASA). MBOSS[4] (University of Arizona) and OOPSS[5] (University of Maryland) are examples of research codes.

Whereas the theoretical basis of MSA for rigid bodies has been well established, a number of improvements have been suggested that would enhance the applicability and efficiency of MSA. One such improvement is to use an object-oriented architecture as the basis for MSA computer programs,[6] to simplify the program structure, improve maintainability, and simplify program expansion. Another suggested improvement is to develop a unified theoretical basis for MSA that will encompass rigid bodies, elastic bodies, and bodies with an arbitrary number of generalized coordinates. The objective of this paper is to investigate the use of Hamilton's weak principle (HWP) as the unifying theoretical basis and to evaluate its impact on obtaining numerical solutions.

Derivation and Solution of the System Equations

Two basic approaches may be used to form the equations of motion and constraint equations for simulation environments such as the one just described. The first approach, known as the maximum coordinate set formulation, results in a large set of differential and algebraic equations (DAEs). These equations include all of the independent and dependent coordinates in the system. An alternative approach, known as the minimum coordinate set approach, produces a much smaller set of differential equations that includes only the independent coordinates.

In a maximum coordinate set formulation, the differential equations of motion of each body in the system are expressed in terms of a basic, often Cartesian, coordinate set. The constraint equations, which are usually algebraic, are then appended to the equations of motion by Lagrange multipliers, resulting in a set of equations that includes all of the independent and dependent coordinates. Assembly of maximum coordinate set equations is relatively easy because the equations of motion for each body and the constraint equations for each joint can be generated independently. This formulation is the foundation for many commercial MSA codes, such as ADAMS[1] and DADS.[2]

The minimum coordinate set formulation assembles the equations of motion in a manner such that only independent generalized coordinates appear in the equations. The number of generalized coordinates and the number of equations are exactly equal to the number of independent system degrees of freedom. Equations of motion that are assembled and solved using a minimum coordinate set incur their major computational costs during the assembly process. The additional expense in assembly results from the necessity for eliminating the dependent coordinates. This operation may be accomplished by selecting a set of generalized coordinates during the derivation of the equations of motion that results in a minimum coordinate set. Alternatively, the equations of motion may be transformed to a minimum coordinate set using the constraint equations. An example of a code that reduces the full set of differential equations to a minimum coordinate set is MBOSS,[4] which was developed at the University of Arizona.

Received 13 September 2000; revision received 25 May 2001; accepted for publication 29 May 2001.

*Associate Professor, Department of Aerospace Engineering; dkunz@odu.edu. Associate Fellow AIAA.

When the equations of motion and constraint equations for a system of interconnected components are developed in maximum coordinate set form, a system of DAEs is the result. The most straightforward approach for obtaining a solution to these equations is to integrate them directly. Although this approach is straightforward, it entails significant mathematical sophistication because the DAEs constitute a stiff system of equations. Algorithms for obtaining solutions to stiff systems, such as the kth-order Gear algorithms,[7] have been developed and are in wide use. However, these algorithms lack error control and can be sensitive to the size of time steps and tolerances. Other direct-integration algorithms that are commonly used include predictor and predictor/corrector methods such as Adams–Bashforth and Adams–Moulton (see Ref. 2). Alternative approaches that have been developed to integrate the DAEs are the constraint violation stabilization method,[2] the generalized coordinate partitioning method,[2] hybrid algorithms,[8] and backward Euler discretization, for example, DASSL.[9] A common criticism of all of these algorithms is that they are not sufficiently robust and may fail to produce a solution for some configurations. The author has had this experience while attempting to perform simulations of complex mechanical systems using a commercial multibody analysis code.

In terms of algorithmic sophistication, the solution of a system of equations in minimum coordinate set form lies at the opposite end of the spectrum from obtaining solutions for a large set of DAEs. For rigid bodies, these equations are simply a set of ordinary differential equations, which can be solved using much simpler techniques, such as Runge–Kutta with fixed or adaptive time steps. There are (at least) two methods by which the equations of motion can be derived as a minimum coordinate set. One method is to identify the independent degrees of freedom for the mechanism and then to derive the equations using those degrees of freedom as the generalized coordinates. The use of this approach requires that a new set of equations be derived for each mechanism being analyzed. Another approach is to assemble the equations of motion in maximum coordinate set form and then identify a transformation that converts the equations into minimum coordinate set form. This method is similar to generalized coordinate partitioning, except that the transformation is valid throughout the simulation. When applied to open-loop systems, the transformation is quite easy to implement, but is much more difficult when applied to closed-loop systems.

To realize the small computational cost afforded by assembly in maximum coordinate set form, this investigation will adopt that methodology. It will also introduce an approach for obtaining a solution of the governing equations that is robust and efficient.

Hamilton's Principle and Hamilton's Law of Varying Action

Hamilton's principle is well known in the scientific literature as a preferred means for deriving the differential equations of motion for dynamic systems. However, Hamilton's principle cannot be used for direct calculations of dynamic system response (initial value problems) because it applies only to stationary systems. For an initial value problem, the initial conditions are known, but the final conditions are not, thus making the system nonstationary.

In the mid-1970s, Bailey[10–12] resurrected Hamilton's law of varying action and showed that it could be used with great accuracy to obtain direct solutions for initial value problems. Baruch and Riff[13] further developed the underlying principles of Hamilton's law and obtained numerical solutions using time finite elements.[14] The principal advantage of using Hamilton's law in lieu of Hamilton's principle is that the intermediate step of deriving the differential equations of motion is eliminated. In addition, the equations resulting from Hamilton's law are algebraic equations, which are easier to solve than the differential equations obtained from Hamilton's principle.

The fundamental reason why Hamilton's law can be used to obtain accurate direct solutions, whereas Hamilton's principle cannot, is that natural boundary conditions (spatial and temporal) are included explicitly in the variational equation. The numerical accuracy of the solution and stability of the solution algorithm is highly dependent on the boundary conditions that are contained in the variational equation. HWP uses a mixed formulation (generalized displacements and forces) to make all boundary conditions natural, thereby greatly improving the characteristics of the numerical solution. For obtaining numerical solutions of dynamic system response,[15,16] HWP has been shown to be a powerful alternative to solving sets of differential equations.

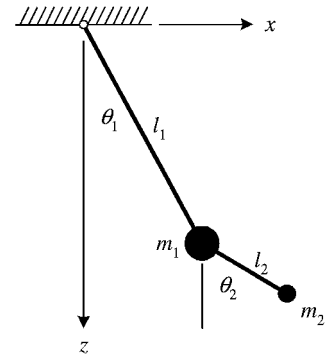

Fig. 1 Double pendulum.

This investigation uses HWP to derive the governing equations. The constraint equations are appended to the body equations using Lagrange multipliers. A simple dynamic system that includes all of the necessary components of MSA is used to demonstrate the effectiveness of this approach. Simulations using the HWP method are then compared to the reference solution, which is obtained from a minimum coordinate set model.

Planar Double Pendulum

To demonstrate that HWP presents a powerful method for numerical simulation of multibody systems, a simple dynamic system that exhibits complex dynamics was selected. The planar double pendulum is a conservative system with only two degrees of freedom (Fig. 1), yet it may be subject to chaotic motion.

Pendulum Bobs

In this analysis, each pendulum bob is modeled as a point mass having two translational coordinates, x and z. The kinetic energy of the double pendulum may be written in terms of the velocities of the pendulum bobs:

$$T = \tfrac{1}{2}m_1\left(\dot{x}_1^2 + \dot{z}_1^2\right) + \tfrac{1}{2}m_2\left(\dot{x}_2^2 + \dot{z}_2^2\right) \tag{1}$$

Alternatively, the kinetic energy may be defined in terms of momentum, where

$$\begin{aligned} p_1 &= m_1\dot{x}_1 \\ q_1 &= m_1\dot{z}_1 \\ p_2 &= m_2\dot{x}_2 \\ q_2 &= m_2\dot{z}_2 \end{aligned} \quad \text{or} \quad \{\rho\} = \begin{bmatrix} m_1 & 0 & 0 & 0 \\ 0 & m_1 & 0 & 0 \\ 0 & 0 & m_2 & 0 \\ 0 & 0 & 0 & m_2 \end{bmatrix} \{\dot{\xi}\} \tag{2}$$

The gravitational forces acting on the pendulum bobs may be incorporated by calculating the potential energy of the system or by considering them to be generalized forces $\boldsymbol{Q}$, which act on the pendulum bobs. The latter approach is used herein:

$$\boldsymbol{Q} = \begin{Bmatrix} 0 \\ m_1 g \\ 0 \\ m_2 g \end{Bmatrix} \tag{3}$$

When the definitions in Eqs. (2) are used, the Hamiltonian of the planar double pendulum can be defined in terms of displacements and momenta. From this point forward in this development, the displacements $\boldsymbol{\xi}$ and momenta $\boldsymbol{\rho}$ are considered to be completely independent quantities:

$$H = \tfrac{1}{2}\left[\left(p_1^2 + q_1^2\right)/m_1 + \left(p_2^2 + q_2^2\right)/m_2\right] \tag{4}$$

Once the Hamiltonian, the generalized forces, the momenta, and the displacements have been defined, HWP can be written as follows:

$$\int_{t_i}^{t_f} [\delta\dot{\boldsymbol{\rho}}^T\boldsymbol{\xi} - \delta\dot{\boldsymbol{\xi}}^T\delta\boldsymbol{\rho} - \delta H + \delta\boldsymbol{\xi}^T\boldsymbol{Q}]\,\mathrm{d}t - \delta\boldsymbol{\xi}^T\boldsymbol{\rho}\Big|_{t_i}^{t_f} + \delta\boldsymbol{\rho}^T\boldsymbol{\xi}\Big|_{t_i}^{t_f} = 0 \tag{5}$$

As described in Ref. 17, Eq. (5) is a mixed formulation because it contains independent variations of both displacements and

momenta. All of the boundary conditions are natural and are enforced by the variational equation for unconstrained variations. These equations are sufficient only to describe the unconstrained, planar motions of the pendulum bobs. To model the double pendulum, the constraints on the pendulum bobs must also be considered.

Constraint Equations

Each of the pendulum bobs has two displacement coordinates. Because a mixed formulation (displacements and momenta) was used to derive the equations of motion, each pendulum bob also has two momentum coordinates. This means that each pendulum bob must have both displacement and momentum constraint equations.

The displacement constraints for each pendulum bob state that the bob must travel in a circular arc relative to the hinge. Therefore, the displacement constraint equations can be written as

$$f_1 = x_1^2 + z_1^2 - l_1^2 = 0$$

$$f_2 = (x_2 - x_1)^2 + (z_2 - z_1)^2 - l_2^2 = 0 \tag{6}$$

The momentum constraint equations for each pendulum bob state that the velocity vector of the bob must be perpendicular to the position vector of the bob relative to the hinge. The momentum equations are written as

$$g_1 = x_1(p_1/m_1) + z_1(q_1/m_1) = 0$$

$$g_2 = (x_2 - x_1)(p_2/m_2 - p_1/m_1) + (z_2 - z_1)(q_2/m_2 - q_1/m_1) = 0 \tag{7}$$

The displacement and momentum constraints are incorporated into Eq. (5) using Lagrange multipliers as follows:

$$\int_{t_i}^{t_f} \left[\delta\dot{\boldsymbol{\rho}}^T\boldsymbol{\xi} - \delta\dot{\boldsymbol{\xi}}^T\delta\boldsymbol{\rho} - \delta H + \delta\boldsymbol{\xi}^T\boldsymbol{Q} + \delta f_1\lambda_1 + \delta f_2\lambda_2 + \delta g_1\mu_1 + \delta g_2\mu_2\right] \mathrm{d}t - \delta\boldsymbol{\xi}^T\boldsymbol{\rho}\Big|_{t_i}^{t_f} + \delta\boldsymbol{\rho}^T\boldsymbol{\xi}\Big|_{t_i}^{t_f} = 0 \tag{8}$$

A complete description of the double pendulum problem is then obtained by appending the four constraint equations to Eq. (8).

Discretization

The selection of the shape functions for the discretization of Eq. (8) is constrained by the orders of the derivatives of the independent variables. One of the advantages of the mixed formulations is that the shape functions can be very simple. Because Eq. (8) contains time derivatives of $\delta\boldsymbol{\xi}$ and $\delta\boldsymbol{\rho}$, those functions must be continuous and piecewise differentiable. There are no time derivatives of $\boldsymbol{\xi}$ and $\boldsymbol{\rho}$, and so their shape functions need only be piecewise continuous. In addition, the displacements and momenta and the variations of the displacements and momenta are mutually independent, and so their shape functions need not be related.[18]

The interval between t_i and t_f may be divided into N time elements (t_n, $n = 0, \ldots, N$), and a nondimensional time τ may be defined:

$$\tau = (t - t_i)/(t_f - t_i) = (t - t_i)/\Delta t \tag{9}$$

For the variations of the displacements and momenta, linear shape functions may be defined as follows:

$$\delta\boldsymbol{\xi} = \delta\boldsymbol{\xi}_n(1 - \tau) + \delta\boldsymbol{\xi}_{n+1}\tau, \qquad \delta\boldsymbol{\rho} = \delta\boldsymbol{\rho}_n(1 - \tau) + \delta\boldsymbol{\rho}_{n+1}\tau \tag{10}$$

For the displacements and momenta, the shape functions are merely constants,

$$\boldsymbol{\xi} = \begin{cases} \hat{\boldsymbol{\xi}}_n & \tau = 0 \\ \bar{\boldsymbol{\xi}}_n & 0 < \tau < 1 \\ \hat{\boldsymbol{\xi}}_{n+1} & \tau = 1 \end{cases}, \qquad \boldsymbol{\rho} = \begin{cases} \hat{\boldsymbol{\rho}}_n & \tau = 0 \\ \bar{\boldsymbol{\rho}}_n & 0 < \tau < 1 \\ \hat{\boldsymbol{\rho}}_{n+1} & \tau = 1 \end{cases} \tag{11}$$

Equations (9–11) may now be substituted into Eq. (8) and the constraint equations. It is easily shown that the barred quantities can be eliminated, along with eight equations, according to the following equations:

$$\bar{\boldsymbol{\xi}}_n = \tfrac{1}{2}(\hat{\boldsymbol{\xi}}_n + \hat{\boldsymbol{\xi}}_{n+1}), \qquad \bar{\boldsymbol{\rho}}_n = \tfrac{1}{2}(\hat{\boldsymbol{\rho}}_n + \hat{\boldsymbol{\rho}}_{n+1}) \tag{12}$$

The resulting set of eight equations, plus the four constraint equations, yield an implicit time-marching algorithm that can be used to solve the initial value problem. At each time step, the 12 unknowns in the equations are the $\hat{\boldsymbol{\xi}}_{n+1}$, $\hat{\boldsymbol{\rho}}_{n+1}$, plus the 4 Lagrange multipliers. The quantities $\hat{\boldsymbol{\xi}}_n$ and $\hat{\boldsymbol{\rho}}_n$ are known at each time step, based on the solution for the previous time step.

Generalized Multibody Architecture

The derivation of the 12 governing, algebraic equations, as described earlier, does not immediately suggest a methodology for developing a simulation capability that can address generalized multibody systems. However, if one looks closely at the structure of the equations, a very definite pattern appears. This pattern is shown in Table 1, where the terms in the equations are separated according to their origin. The body terms come from the first three terms of the integrand in Eq. (8) plus the trailing terms. The last four terms of the integrand are the sources of the joint terms; the fourth term is the source of the force terms. In general, it can be shown that the first three terms in the integrand and the trailing terms will always produce the terms that define the body dynamics. Similarly, the terms in the integrand that come from the constraint equations will always produce the joint contributions. As long as all of the external forces are modeled as generalized forces, that is, not as components of kinetic or potential energy, the generalized force term will generate the force contributions.

The equations for the double pendulum can be easily assembled by making a new table for the upper pendulum, then superimposing that table on Table 1. The upper pendulum table is constructed by changing all of the 1 subscripts in Table 1 to 0 and all of the 2 subscripts to 1. Because the hinge of the upper pendulum is fixed, equations and variables with a subscript 0 may be eliminated. The constraint equations can be handled in a similar manner.

The full set of 12 nonlinear, algebraic equations that govern the motion of the double pendulum may be found in Appendix A. These equations may be viewed as a set of residual equations that are

Table 1 Lower pendulum residual equations

Equation	Body	Joint	Force
δx_1		$-\lambda_2(\bar{x}_2 - \bar{x}_1)\Delta t - \frac{1}{2}\mu_2(\bar{p}_2 - \bar{p}_1)\Delta t$	
δz_1		$-\lambda_2(\bar{z}_2 - \bar{z}_1)\Delta t - \frac{1}{2}\mu_2(\bar{q}_2 - \bar{q}_1)\Delta t$	
δp_1		$-\frac{1}{2}\mu_2(\bar{x}_2 - \bar{x}_1)\Delta t$	
δq_1		$-\frac{1}{2}\mu_2(\bar{z}_2 - \bar{z}_1)\Delta t$	
δx_2	$\bar{p}_2 - \hat{p}_{2f}$	$\lambda_2(\bar{x}_2 - \bar{x}_1)\Delta t + \frac{1}{2}\mu_2(\bar{p}_2 - \bar{p}_1)\Delta t$	
δz_2	$\bar{q}_2 - \hat{q}_{2f}$	$\lambda_2(\bar{z}_2 - \bar{z}_1)\Delta t + \frac{1}{2}\mu_2(\bar{q}_2 - \bar{q}_1)\Delta t$	$\frac{1}{2}gm_2\Delta t$
δp_2	$-\bar{x}_2 + \hat{x}_{2f} - \frac{1}{2}(\bar{p}_2/m_2)\Delta t$	$\frac{1}{2}\mu_2(\bar{x}_2 - \bar{x}_1)\Delta t$	
δq_2	$-\bar{z}_2 + \hat{z}_{2f} - \frac{1}{2}(\bar{q}_2/m_2)\Delta t$	$\frac{1}{2}\mu_2(\bar{z}_2 - \bar{z}_1)\Delta t$	

satisfied when the values of the unknowns drive the left-hand sides to zero.

Numerical Evaluation

To evaluate multibody system analysis based on HWP, benchmark cases based on a minimum coordinate set formulation were created for the double pendulum problem. HWP solutions for these cases were then compared with the benchmark solutions.

Benchmark Cases

To establish a benchmark, against which time history solutions obtained by solving the equations in Appendix A can be compared, the equations of motion for the planar double pendulum were cast in their minimum coordinate set form. Because these equations can easily be derived using Hamilton's principle or Lagrange's equations, the derivations are not discussed herein. The resulting first-order ordinary differential equations (ODEs) are

$$(m_1 + m_2)l_1^2\dot{\omega}_1 + m_2 l_1 l_2 \dot{\omega}_2 \cos(\theta_1 - \theta_2)$$
$$= -m_2 l_1 l_2 \omega_2^2 \sin(\theta_1 - \theta_2) - g(m_1 + m_2) l_1 \sin\theta_1$$
$$m_2 l_1 l_2 \dot{\omega}_1 \cos(\theta_1 - \theta_2) + m_2 l_2^2 \dot{\omega}_2$$
$$= m_2 l_1 l_2 \omega_1^2 \sin(\theta_1 - \theta_2) - g m_2 l_2 \sin\theta_2$$
$$\dot{\theta}_1 = \omega_1, \qquad \dot{\theta}_2 = \omega_2 \tag{13}$$

For the purposes of this investigation, the Mathematica® implementation of the implicit Adams method (see Ref. 19) with order between 1 and 12 was used to obtain the time history solution of Eqs. (13). The accuracy goal for the algorithm was set to 10^{-7}, and the precision goal was set to infinity. Solutions obtained using this approach are henceforth called the ODE solutions.

First, the accuracy of the ODE solution was determined by comparing it to an exact benchmark solution constructed using the method described in Ref. 20. An initial value solution for the set of ODEs over a representative time period was obtained using the Adams method. Solution functions approximating the solutions of the differential equations were constructed from orthogonal Chebyshev polynomials. When inverse dynamics is used, these functions were then used to derive perturbation functions that were appended to the differential equations, thus making the solution functions exact solutions of the modified differential equations.

For the baseline double pendulum parameters defined in Table 2, the natural frequencies are 2.94 and 1.29 rad/s, and the corresponding periods are 2.14 and 4.86 s, respectively. Therefore, the longer time period (4.86 s) was chosen as the period for the initial value problem. Solutions for Eqs. (13) were obtained for the configurations described in Table 2. Chebyshev polynomials of order 30 were used to construct the solution functions. The accuracy of the Adams method for this problem was then determined based on the L_2 norms of the exact solution functions and the solutions of the modified differential equations over the period. For the upper bob, the L_2 norm was 3.79×10^{-10}; the L_2 norm for the lower bob was 1.03×10^{-9}. The accuracy of the Adams method compared to an exact benchmark solution similar to the double pendulum problem was, therefore, validated, and the ODE solution can confidently be used to create benchmark cases.

Nonlinear Response Case

The first benchmark case is one for which the response of the double pendulum is known to be nonlinear. The pendulum parameters for this case were identical to those in Table 2, and the simulation was run for 500 s. For the purposes of qualitative comparison with subsequent calculations, phase plane plots (Figs. 2 and 3) were created for the upper and lower pendulum bobs, as well as a Poincaré map (Fig. 4) of the pendulum response. For Fig. 4 and all subsequent Poincaré maps, the plotted points were obtained by recording the angular position and angular velocity of the lower pendulum bob as the upper bob crossed the vertical plane while going right to left (Fig. 1). Figure 4 contains 1942 points, which were obtained from a simulation of 10,000 s. Note that the Poincaré map is elliptical, indicating that the response is periodic.

Table 2 Planar double pendulum baseline parameters

Parameter	Upper	Lower
Bob mass, kg	2	1
Rod length, m	5	2
Initial position, deg	30	30
Initial velocity, rad/s	0	0
Gravity, m/s^2	9.807	——

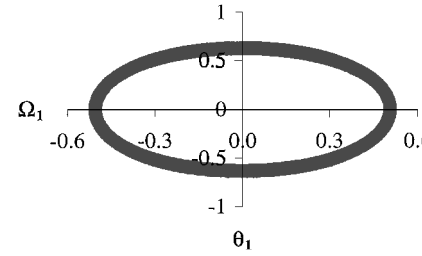

Fig. 2 Nonlinear baseline case: phase plane for upper pendulum bob.

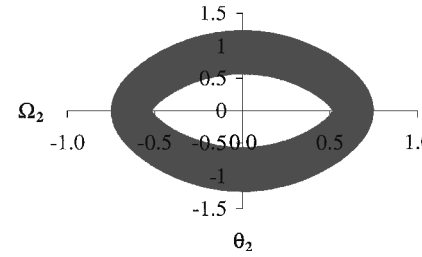

Fig. 3 Nonlinear baseline case: phase plane for lower pendulum bob.

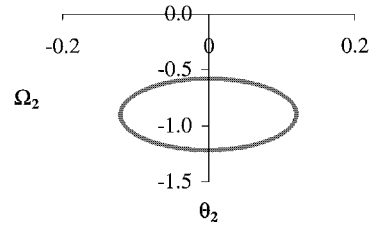

Fig. 4 Nonlinear baseline case: Poincaré map.

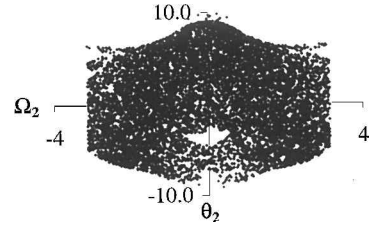

Fig. 5 Chaotic baseline case: Poincaré map.

Chaotic Response Case

The second benchmark case is one for which the response of the double pendulum is known to be chaotic. The pendulum parameters for this case are identical to those in Table 2, except that the initial positions of the upper and lower pendulum bobs are at 90 deg. As in the first benchmark case, the simulation was run for 500 s. As verification of the chaotic nature of the response, sensitive dependence on initial conditions was observed for changes in initial conditions as small as 0.0001 deg. Figure 5 is the Poincaré map for the chaotic benchmark case. This plot contains 9769 points, which were obtained as discussed earlier, from a simulation of 50,000 s in duration. Figure 5 will be used for qualitative comparisons with other solution methods.

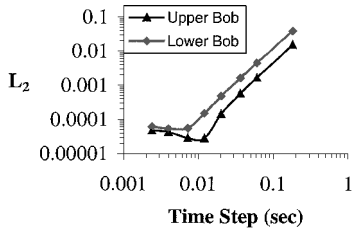

Fig. 6 HWP solution time step size.

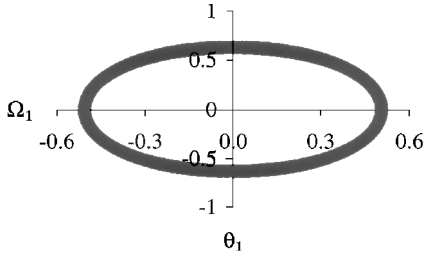

Fig. 7 Nonlinear HWP solution: phase plane for upper pendulum bob.

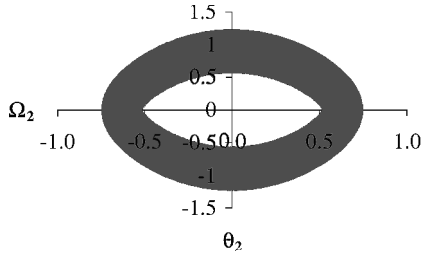

Fig. 8 Nonlinear HWP solution: phase plane for lower pendulum bob.

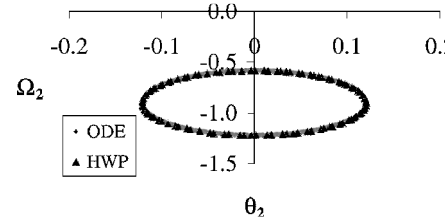

Fig. 9 Nonlinear response: Poincaré map.

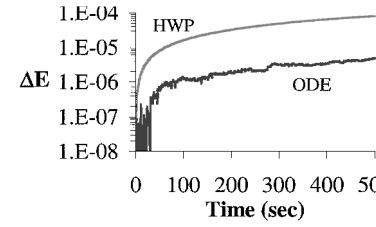

Fig. 10 HWP vs ODE: nonlinear response fractional energy change.

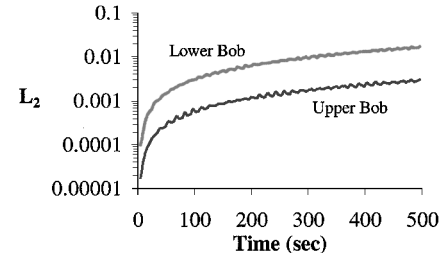

Fig. 11 L_2 norm for HWP nonlinear response.

HWP vs ODE

The equations of motion derived using HWP are nonlinear, algebraic equations (Appendix A). Therefore, a variety of algorithms are available to obtain solutions for the equations at each time step. For this investigation, an object-oriented implementation of the Newton–Raphson method (see Ref. 21) was used because of its stability and ease of programming. The absolute tolerance for convergence, which is equivalent to the accuracy goal for the ODE solution, was also set to 10^{-7}.

To determine a suitable time step for the HWP simulations, the nonlinear benchmark case was run for a number of different time steps over a period of 4.86 s. A plot of the L_2 norm (compared to the benchmark solution) vs the time step is shown in Fig. 6. Based on these results, a time step of 0.01 s was selected for all subsequent simulations.

The solutions obtained for the nonlinear and chaotic benchmark cases using the HWP method were compared to the ODE solutions both qualitatively and quantitatively. Qualitatively, comparisons between the two solution methods of the phase plane plots for the upper and lower pendulum bobs, as well as comparisons of the Poincaré maps, can be made. Quantitative comparisons were made between the fractional energy change calculated for each of the two solution methods and from the L_2 norm of the HWP solution using the ODE solution as the baseline.

HWP vs ODE: Nonlinear Response

Qualitative assessments of the HWP solution for the case of nonlinear response using the planar double pendulum can be made by comparing the phase plane plots for the upper pendulum bob (Figs. 2 and 7) and for the lower pendulum bob (Figs. 3 and 8). For all intents and purposes, the curves are identical. In addition, a comparison of the Poincaré maps is shown in Fig. 9. Both the ODE solution (10,000-s simulation time) and HWP solution (500-s simulation time) are plotted together, and the HWP points fall on top of the ODE points.

The fractional energy change is defined as being the absolute value of the difference between the total energy at a time step and the total energy at the start of the simulation, divided by the total energy at the start of the simulation. Figure 10 compares the energy change during simulations performed using both solution methods. Clearly, the ODE solution is superior to the HWP solution according to this metric. However, the energy change in the HWP solution after 500 s is still less than 1/100th of 1%, which should be sufficiently accurate for most applications. In addition, the slopes of the two curves show that the total energy for both solution methods is changing at approximately the same rate.

In Fig. 11, the L_2 norm is plotted for the HWP solution, using the ODE solution as the basis for comparison. The time interval over which the norm is calculated is 4.86 s. Again, the HWP solution does not deliver the level of accuracy exhibited by the ODE solution, when compared to the earlier exact benchmark case. However, it is evident that the accuracy of the HWP solution is sufficient for the duration of this simulation (500 s) because the eye cannot discern the difference between the time history responses produced by the two methods. Figure 11 also shows that the norm is growing with time, but at a rate that is consistent with the accuracy goal enforced in the Newton–Raphson algorithm.

HWP vs ODE: Chaotic Response

In a manner similar to the response calculated by the ODE method for the chaotic case, the HWP method exhibits sensitive dependence on initial conditions. Therefore, although qualitative comparisons of the phase plane plots and Poincaré maps can be made, as well as a quantitative comparison of the fractional energy change, it makes no sense to attempt to calculate the L_2 norm of the HWP solution using the ODE solution as the baseline. The numerical differences that result from the different solution algorithms are more than enough to cause sensitive dependence to give divergent solutions.

Figure 12 is the Poincaré map of the HWP solution for a simulation that ran for 50,000 s. There are 9750 point plotted in Fig. 12. A comparison of Fig. 12 with the Poincaré map for the ODE solution (Fig. 5) shows remarkable qualitative agreement. The most notable features that the two Poincaré maps have in common, in addition to the overall similarity in shape, are the smile-shaped area in the lower half of the form and the wedge-shaped cutouts in upper right and upper left corners. In addition, both maps have a roughly semicircular cutout at the very bottom of the form. It can, therefore, be

Table 3 Run time comparison

Case	Fraction of real time
ODE nonlinear	0.0043
ODE chaotic	1.25
HWP nonlinear	0.29
HWP chaotic	0.45

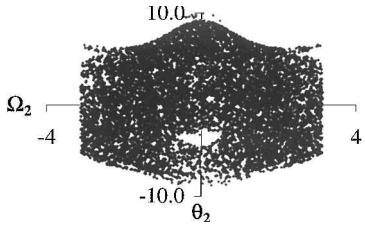

Fig. 12 Chaotic HWP solution: Poincaré map.

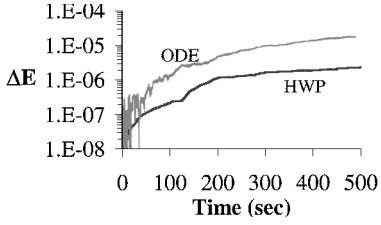

Fig. 13 HWP vs ODE: chaotic response fractional energy change.

concluded that the results of the HWP solution are in qualitative agreement with the baseline ODE solution.

A quantitative comparison of the HWP solution and the ODE baseline solution is made in Fig. 13. Figure 13 compares the fractional energy change for the two solution methods for the first 500 s of the chaotic simulation. In contrast to the nonlinear, periodic case discussed earlier, the HWP method actually conserves energy better than the ODE baseline for the chaotic case and, toward the end of the simulation record, the rate of energy change is somewhat better for the HWP method. Thus, it can be concluded that, quantitatively, the HWP solution compares well with the ODE baseline solution.

Computational Efficiency

One final item of interest is the computational efficiency of the HWP solution method. All of the calculations presented herein were performed on a computer equipped with a 600-MHz Pentium III processor and 196 MB of RAM memory. Using real time as the basis for comparison, Table 3 compares the run times for the cases discussed.

Given that the double pendulum problem, as formulated herein, has relatively few equations, 12, it would be expected that simulations of a complex dynamic system would have significantly longer run times. Also, note that halving the time step for the HWP method does not result in an exact doubling of the run time. This is probably because the solution obtained at a particular time step is a better initial guess for the solution at the following step. Thus, fewer iterations are required for the Newton–Raphson method to converge to a solution.

Conclusions

The algebraic equations of motion for a planar double pendulum were derived in maximum coordinate set form using HWP. These equations result in an implicit time-marching algorithm that can be used to solve an initial value problem. The planar double pendulum is a particularly simple multibody system, consisting only of rigid bodies and hinge joints, but it does demonstrate most generic multibody components (except prescribed motion). Based on the structure of the equations, a generalized methodology for the assembly of multibody systems has been deduced and may be applied to other types of bodies, joints, and forces.

Validation of simulations using the HWP method was performed in three steps. First, results for nonlinear, periodic motion produced by the ODE method were validated against an exact solution of a similar set of equations. Then, simulations for nonlinear, periodic motion obtained using the HWP method were compared to baseline simulations performed using the ODE method. Finally, simulations for chaotic motion obtained using the HWP method were compared to ODE baseline simulations.

Qualitative comparisons of the HWP simulations with the baseline ODE simulations for a configuration exhibiting nonlinear, periodic response exhibited excellent agreement. Phase plane plots of the upper and lower pendulum bobs, as well as the Poincaré map, were virtually identical. The HWP simulations also showed excellent quantitative agreement with the baseline ODE simulations. For a simulation time of 500 s, the L_2 norms for the HWP results (compared to the ODE results) were less than 0.004 and 0.02 for the upper and lower bobs, respectively. In addition, the rate of change in total system energy for both solutions methods was equivalent.

For the simulations of chaotic response, the HWP results also exhibited excellent qualitative and quantitative agreement with the baseline ODE results. Qualitatively, the Poincaré maps of HWP and ODE simulations, each of which contain more than 9700 points, show remarkable similarity. As in the case of linear, periodic motion, the rate of change in total system energy indicated good quantitative agreement between the HWP and ODE simulation results.

Note that the DAEs for the planar double pendulum (Appendix B) could be discretized using constant shape functions for the variational quantities and linear shape functions for the state variables. The resulting equations would permit a time finite element solution. For this dynamic system, it turns out that the time finite element equations and the HWP equations are identical.

Appendix A: Equations of Motion from HWP

The following eight equations are the residual equations derived from HWP:

$$\bar{p}_1 - \hat{p}_{1f} + \lambda_1 \bar{x}_1 \Delta t - \lambda_2(\bar{x}_2 - \bar{x}_1)\Delta t + \tfrac{1}{2}\mu_1(\bar{p}_1/m_1)\Delta t - \tfrac{1}{2}\mu_2[(\bar{p}_2/m_2) - (\bar{p}_1/m_1)]\Delta t = 0$$

$$\bar{q}_1 - \hat{q}_{1f} + \lambda_1 \bar{z}_1 \Delta t - \lambda_2(\bar{z}_2 - \bar{z}_1)\Delta t + \tfrac{1}{2}\mu_1(\bar{q}_1/m_1)\Delta t - \tfrac{1}{2}\mu_2[(\bar{q}_2/m_2) - (\bar{q}_1/m_1)]\Delta t + \tfrac{1}{2}gm_1\Delta t = 0$$

$$-\bar{x}_1 + \hat{x}_{1f} - \tfrac{1}{2}(\bar{p}_1/m_1)\Delta t + \tfrac{1}{2}(\mu_1/m_1)\bar{x}_1\Delta t - \tfrac{1}{2}(\mu_2/m_1)(\bar{x}_2 - \bar{x}_1)\Delta t = 0$$

$$-\bar{z}_1 + \hat{z}_{1f} - \tfrac{1}{2}(\bar{q}_1/m_1)\Delta t + \tfrac{1}{2}(\mu_1/m_1)\bar{z}_1\Delta t - \tfrac{1}{2}(\mu_2/m_1)(\bar{z}_2 - \bar{z}_1)\Delta t = 0$$

$$\bar{p}_2 - \hat{p}_{2f} + \lambda_2(\bar{x}_2 - \bar{x}_1)\Delta t + \tfrac{1}{2}\mu_2[(\bar{p}_2/m_2) - (\bar{p}_1/m_1)]\Delta t = 0$$

$$\bar{q}_2 - \hat{q}_{2f} + \lambda_2(\bar{z}_2 - \bar{z}_1)\Delta t + \tfrac{1}{2}\mu_2[(\bar{q}_2/m_2) - (\bar{q}_1/m_1)]\Delta t + \tfrac{1}{2}gm_2\Delta t = 0$$

$$-\bar{x}_2 + \hat{x}_{2f} - \tfrac{1}{2}(\bar{p}_2/m_2)\Delta t + \tfrac{1}{2}(\mu_2/m_2)(\bar{x}_2 - \bar{x}_1)\Delta t = 0$$

$$-\bar{z}_2 + \hat{z}_{2f} - \tfrac{1}{2}(\bar{q}_2/m_2)\Delta t + \tfrac{1}{2}(\mu_2/m_2)(\bar{z}_2 - \bar{z}_1)\Delta t = 0$$

The following four equations are the residual equations derived from the constraint equations:

$$\left(\hat{x}_{1f}^2 + \hat{z}_{1f}^2\right) - \left(\hat{x}_{1i}^2 + \hat{z}_{1i}^2\right) = 0$$

$$\left[(\hat{x}_{2f} - \hat{x}_{1f})^2 + (\hat{z}_{2f} - \hat{z}_{1f})^2\right] - \left[(\hat{x}_{2i} - \hat{x}_{1i})^2 + (\hat{z}_{2i} - \hat{z}_{1i})^2\right] = 0$$

$$\hat{x}_{1f}(\hat{p}_{1f}/m_1) + \hat{z}_{1f}(\hat{q}_{1f}/m_1) = 0$$

$$(\hat{x}_{2f} - \hat{x}_{1f})(\hat{p}_{2f}/m_2 - \hat{p}_{1f}/m_1) + (\hat{z}_{2f} - \hat{z}_{1f})(\hat{q}_{2f}/m_2 - \hat{q}_{1f}/m_1) = 0$$

Appendix B: Maximum Coordinate Set ODEs

$$\dot{p}_1 - 2\lambda_1 x_1 + 2\lambda_2(x_2 - x_1) - \mu_1(p_1/m_1) + \mu_2(p_2/m_2 - p_1/m_1) = 0$$

$$\dot{q}_1 - 2\lambda_1 z_1 + 2\lambda_2(z_2 - z_1) - \mu_1(q_1/m_1) + \mu_2(q_2/m_2 - q_1/m_1) - gm_1 = 0$$

$$\dot{x}_1 - p_1/m_1 + (\mu_1/m_1)x_1 - (\mu_2/m_1)(x_2 - x_1) = 0$$

$$\dot{z}_1 - q_1/m_1 + (\mu_1/m_1)z_1 - (\mu_2/m_1)(z_2 - z_1) = 0$$

$$\dot{p}_2 - 2\lambda_2(x_2 - x_1) - \mu_2(p_2/m_2 - p_1/m_1) = 0$$

$$\dot{q}_2 - 2\lambda_2(z_2 - z_1) - \mu_2(q_2/m_2 - q_1/m_1) - gm_2 = 0$$

$$\dot{x}_2 - p_2/m_2 + (\mu_2/m_2)(x_2 - x_1) = 0$$

$$\dot{z}_2 - q_2/m_2 + (\mu_2/m_2)(z_2 - z_1) = 0$$

References

[1]Ryan, R. R., "ADAMS: Multibody System Analysis Software," *Multibody Systems Handbook*, edited by W. Scheihlen, Springer-Verlag, Berlin, 1990, pp. 361–402.

[2]Haug, E. J., *Computer Aided Kinematics and Dynamics of Mechanical Systems, Volume 1: Basic Methods*, Allyn and Bacon, Boston, 1989.

[3]Korium, W., Rulka, W., and Eichberger, A., "Recent Enhancements of SIMPACK and Vehicle Applications," EUROMECH 320, European Mechanics Colloquium, June 1994.

[4]Nikravesh, P. E., and Gim, G., "Systematic Construction of the Equations of Motion for Multibody Systems Containing Closed Kinematic Loops," ASME Design Automation Conf., American Society of Mechanical Engineers, 1989.

[5]Sreenath, N., and Krishnaprasad, P. S., "Multibody Simulation in an Object-Oriented Programming Environment," Systems Research Center, SRC TR 88-25, Univ. of Maryland, College Park, MD, 1988.

[6]Kunz, D. L., "An Object-Oriented Approach to Multibody Systems Analysis," *Computers and Structures*, Vol. 69, No. 2, 1998, pp. 209–217.

[7]Gear, C. W., *Numerical Initial Value Problems in Ordinary Differential Equations*, Prentice–Hall, Englewood Cliffs, NJ, 1971, Chap. 11.

[8]Park, T., "A Hybrid Constraint Stabilization-Generalized Coordinate Partitioning Method for Machine Dynamics," *Journal of Mechanisms, Transmissions, and Automation in Design*, Vol. 108, No. 2, 1986, pp. 211–216.

[9]Brenan, K. E., Campbell, S. L., and Petzold, L. R., *Numerical Solution of Initial-Value Problems in Differential-Algebraic Equations*, North-Holland, Amsterdam, 1989, Chap. 5.

[10]Bailey, C. D., "A New Look at Hamilton's Principle," *Foundations of Physics*, Vol. 5, No. 3, 1975, pp. 433–451.

[11]Bailey, C. D., "Application of Hamilton's Law of Varying Action," *AIAA Journal*, Vol. 13, No. 9, 1975, pp. 1154–1157.

[12]Bailey, C. D., "Exact and Direct Analytical Solutions to a Vibrating System with Discontinuties," *Journal of Sound and Vibration*, Vol. 44, No. 1, 1976, pp. 15–25.

[13]Baruch, M., and Riff, R., "Hamilton's Principle, Hamilton's Law—6^n Correct Formulations," *AIAA Journal*, Vol. 20, No. 5, 1982, pp. 687–692.

[14]Riff, R., and Baruch, M., "Time Finite Element Discretization of Hamilton's Law of Varying Action," *AIAA Journal*, Vol. 22, No. 9, 1984, pp. 1310–1318.

[15]Borri, M., Ghiringhelli, G. L., Lanz, M., Manteganzza, P., and Merlini, T., "Dynamic Response of Mechanical Systems by a Weak Hamiltonian Formulation," *Computers and Structures*, Vol. 20, Nos. 1–3, 1985, pp. 495–508.

[16]Peters, D. A., and Izadpanah, A., "hp-Version Finite Elements for the Space–Time Domain," *Computational Mechanics*, Vol. 3, No. 2, 1988, pp. 73–88.

[17]Hodges, D. H., and Bless, R. R., "A Weak Hamiltonian Finite Element Method for Optimal Control Problems," *Journal of Guidance, Control, and Dynamics*, Vol. 14, No. 1, 1991, pp. 148–156.

[18]Riff, R., and Baruch, M., "Stability of Time Finite Elements," *AIAA Journal*, Vol. 22, No. 8, 1984, pp. 1171–1173.

[19]Wolfram, S., *The Mathematica Book*, Cambridge Univ. Press, New York, 1996, pp. 886–894.

[20]Junkins, J. L., and Lee, S., "Validation of Finite-Dimensional Approximate Solutions for Dynamics of Distributed-Parameter Systems," *Journal of Guidance, Control, and Dynamics*, Vol. 18, No. 1, 1995, pp. 87–95.

[21]Perry, M. L., "A Reusable Nonlinear System Solver, Part 1," *C/C++ Users Journal*, Vol. 18, No. 6, 2000, pp. 22–31.

A. Berman
Associate Editor